

Communications

Improving Calibration of 3-D Video Oculography Systems

Kai Schreiber* and Thomas Haslwanter

Abstract—Eye movement recordings with video-based techniques have become very popular, as long as they are restricted to the horizontal and vertical movements of the eye. Reliable measurement of the torsional component of eye movements, which is especially important in the diagnosis and investigation of pathologies, has remained a coveted goal. One of the main reasons is unresolved technical difficulties in the analysis of video-based images of the eye. Based on simulations, we present solutions to two of the primary problems: a robust and reliable calibration of horizontal and vertical eye movement recordings, and the extraction of suitable iris patterns for the determination of the torsional eye position component.

Index Terms—Biomedical image processing, eye movements, image analysis, video-oculography.

I. INTRODUCTION

Recent advances in the understanding of the motor control of eye movements and new findings in the anatomy of the extraocular muscles have greatly increased the interest in a complete three-dimensional (3-D) description of eye position, i.e., of the horizontal, vertical, and torsional component.

Dual search coils have been used successfully to measure all three components [3], [14]. But search-coil recordings are expensive and invasive, limit the measurement duration to about 30 min and may slip on the eye, introducing artifacts [17]. They also cannot be applied to young children, since only one size of coils is available. These difficulties have focused attention on video oculography (VOG): using video images of the eye to measure 3-D eye position. While hardware improvements in recent years have made high-frequency sampling and online analysis available, problems in the data analysis continue to impede the development of a reliable VOG system. Two problems are addressed in this paper:

- a reliable calibration of the measurement setup;
- selection of suitable iral patterns for measuring the torsional component of the eye movement.

One source of problems in VOG systems are errors in target fixation during the calibration process. It has been shown that even healthy subjects show a variability as large as $\pm 0.5^\circ$ (for trained subjects, this can go down as low as $\pm 0.1^\circ$) [12]. These inaccuracies can induce a large variability in the calibration parameters. The most successful approaches to this problem are based on numerical minimization procedures. These procedures use an array of target points at well-defined locations, and calculate the calibration parameters as a best fit to the recorded pupil positions [13]. Efforts to utilize the geometric distortion of the pupil in excentric gaze positions have so far proven ineffective because of the variability of the human pupil [19].

Manuscript received October 14, 2002; revised August 10, 2003. This work was supported by the Swiss National Science Foundation under Grant 3100-063669. Asterisk indicates corresponding author.

*K. Schreiber is with the School of Optometry, University of California at Berkeley, 360 Minor Hall, Berkeley, CA 94720-2020 USA. (e-mail: schreiber@genista.de).

T. Haslwanter is with the ETH/University of Zurich, 8091 Zurich, Switzerland, and Upper Austrian Research, Austria.

Digital Object Identifier 10.1109/TBME.2003.821025

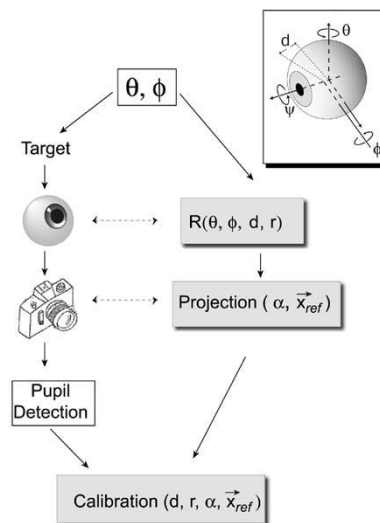


Fig. 1. Steps in calibrating the system. (left column) Presentation of the calibration targets at (θ, ϕ) —Eye movement—Projection into the image plane—Pupil detection. (right column) The shaded boxes indicate the required algorithms. The inset shows the rotation axes of the eye. Note that the axis for horizontal eye movements (by θ) does *not* intersect with the axis for vertical eye movements (by ϕ). The distance between the two is d . Torsional eye movements are described by the rotation about the line of sight (by ψ).

For measuring ocular torsion, i.e., the rotation around the line of sight, features on the eye must be tracked. Most existing systems use a cross correlation of iral patterns to track the torsional movement of the eye [1], [9]. But precision and stability of this technique are highly dependent on the structure of the selected patterns.

Here, we present new algorithms for these two problems. We first describe a stable and reliable method for finding calibration parameters by numerical minimization, and then demonstrate a semi-automatic technique for selecting suitable iral patterns for torsion measurement.

II. METHODS

The left column of Fig. 1 shows the required experimental steps for obtaining calibration data: A physical target, e.g., a laser dot, is presented to the subject at selected locations. While the subject fixates the target, their eye is imaged and the center of the pupil is detected. A number of accurate techniques are available for pupil detection [5], [20].

The right column of Fig. 1 shows the algorithmic representation of the experimental steps. A kinematic model yields the spatial coordinates of the pupil center as a function of eye orientation (θ and ϕ), the eye radius (r), and the axial displacement (d). These pupil-coordinates are then projected into the image plane. The projection has three parameters: the horizontal and vertical position of the eye in the camera image, $\vec{x}_{ref} = (x_{ref}, y_{ref})$, and the rotation of the camera around its optical axis by an angle α . Note that small rotations of the camera about its horizontal and vertical axis have little effect on the accuracy of VOG systems [10].

For our calculations we have used a rectangular, right-handed coordinate system with the x axis pointing forward, the y axis pointing to the left and the z axis pointing up, with the origin in the center of the

eye. Angular positions will be expressed in Helmholtz angles, (ϕ for downward, θ for leftward and ψ for clockwise gaze angles, subject's perspective). For details on the mathematical treatment of three dimensional eye movements see [7].

A. Kinematic Model of Eye Movement

Fry and Hill showed in 1962 that the kinematics of the eye cannot be accounted for by a purely rotational model [4]. Rather, the position of the center of rotation depends on current gaze direction. A good approximation of the actual kinematics is achieved by having the axis for vertical rotations shifted with respect to the axis for horizontal rotations. We call the distance between these two axes the axial displacement d (see inset Fig. 1).

The transformation \mathcal{R} , which describes the location of any point \vec{p} on the surface of the eye after a (Helmholtz) rotation by (θ, ϕ, ψ) around these axes can be written as

$$\mathcal{R} = \mathcal{R}(\vec{p}, \theta, \phi, \psi, d) \quad (1)$$

$$= \begin{pmatrix} d \\ 0 \\ 0 \end{pmatrix} + \mathcal{V}(\phi) \cdot \left(\mathcal{H}(\theta) \cdot \mathcal{T}(\psi) \cdot \vec{p} - \begin{pmatrix} d \\ 0 \\ 0 \end{pmatrix} \right) \quad (2)$$

where $\mathcal{H}(\theta)$, $\mathcal{V}(\phi)$ and $\mathcal{T}(\psi)$ are the standard rotation matrices for rotations around the vertical, horizontal and torsional axis, respectively [7].

For the calibration we define a reference eye position where the center of pupil \vec{p} lies on the x axis, at a distance r from the center of the eye

$$\vec{p} = \begin{pmatrix} r \\ 0 \\ 0 \end{pmatrix}. \quad (3)$$

Using (2), this yields the formula for the pupil position in Helmholtz coordinates

$$\mathcal{R}(\theta, \phi) = \begin{pmatrix} r \cos(\theta) \cos(\phi) + d(1 - \cos(\phi)) \\ r \sin(\theta) \\ -r \cos(\theta) \sin(\phi) + d \sin(\phi) \end{pmatrix}. \quad (4)$$

Note that this does not depend on the torsion ψ , since in this model torsional rotations are performed around the center of the pupil. Wyatt has shown that the pupil center shifts as the pupil contracts or expands [18], adding to the signal noise. Such changes in pupil size occur when illumination changes, but can also occur independent of illumination [16]. Future algorithms should include a fixation sequence with changing illumination that maps the relation of pupil diameter to the location of the center. Under conditions of constant illumination, though, the assumption of a constant pupil center holds well.

B. Optical Transformation

For standard CCD cameras using one lens to focus the image on the CCD chip, a central projection of the eye through the lens onto the image plane is given by

$$\mathcal{P}(\vec{p}) = \begin{pmatrix} \cos(\alpha) & \sin(\alpha) \\ -\sin(\alpha) & \cos(\alpha) \end{pmatrix} \cdot \begin{pmatrix} 0 & \frac{g+r-\mathcal{R}_1}{b} & 0 \\ 0 & 0 & \frac{g+r-\mathcal{R}_1}{b} \end{pmatrix} \mathcal{R}(\theta, \phi) + \vec{x}_{\text{ref}}. \quad (5)$$

\mathcal{R}_1 is the first component of $\mathcal{R}(\theta, \phi)$. This equation assumes that the camera is set up so that pupil and iris are in focus when the eye is in the reference position. b is the distance from the lens to the CCD chip, and g the distance from the lens to the center of the pupil. b can be obtained from the physical setup of the system, and g from b and the properties of the lens. The numerator of the fraction is the actual distance of \vec{p}

from the lens. The first matrix rotates the image, simulating a rotation of the camera around its optical axis by the angle α . Finally the image is re-centered to \vec{x}_{ref} .

C. Combination of Rotation of the Eye, and Projection Into the Image Plane

Combining the two formulas above, we can compute the location of the pupil center in the image plane of the camera as a function of the parameters of the eye (radius r , and axial displacement d), and the location (\vec{x}_{ref}) and orientation (α) of the camera

$$\mathcal{F}(\theta, \phi) = \mathcal{P}(\mathcal{R}(\theta, \phi)). \quad (6)$$

Once the calibration parameters have been determined, we can invert \mathcal{F} to compute gaze direction from pupil image position.

D. Calculation of Calibration Parameters

$\mathcal{F}(\theta, \phi)$ contains five parameters: r and d in \mathcal{R} , both varying between subjects; the two components of \vec{x}_{ref} , and α . The estimate of these parameters should be stable in the face of (natural) variability in the subject's fixations.

We can estimate these parameters by numerically minimizing the error function

$$E(r, d, \vec{x}_{\text{ref}}, \alpha) = \sum_i (\mathcal{F}(\theta_i, \phi_i) - \vec{x}_i)^2 \quad (7)$$

i.e., the squared difference between the model's predicted and the actual pupil image positions.

We tested the stability of this calibration method in simulations. The minimization method used for the simulations was the Levenberg–Marquardt algorithm included in the version 2.0 of the optimization toolbox of the Matlab programming environment.

III. THE MEASURABLE ANGULAR DISTANCE (MAD) CRITERION

Most VOG systems measure ocular torsion by using the "irial signature" approach, where a circular segment of the iris is extracted from the image when the eye is in the reference position. Cross-correlation of this segment with a segment extracted from the same location in a different eye position allows the computation of ocular torsion [8], [9]. With this technique a precise measurement of gaze is required to determine the correct position of the chosen irial signature [8]. The stability of this method also depends strongly on the chosen pattern. Increasing torsion reduces the overlap between the current and reference patterns, eventually resulting in a measurement error. We call the torsional range over which a retinal pattern can be used to measure eye position without this type of error the MAD of this pattern. The technique is described in Fig. 2.

A common practice to choose retinal signatures for torsion measurement is based on the shape of their autocorrelation function, specifically the width of the central peak. We, therefore, compared the results of MAD to the full width at half height of this central peak.

IV. RESULTS

A. Calibration

To test the stability of the suggested calibration algorithms, we simulated calibration sessions. A set of parameters was chosen randomly from the following ranges: $x_{\text{ref}} = 270\text{--}350$, $y_{\text{ref}} = 170\text{--}230$, $r = 840\text{--}880$, $d = 19.5\text{--}20.5$ (these values are all in pixels and correspond to a common optical setup, with 640×400 resolution, the pupil in the center and the image of the eye slightly larger than the screen), and $\alpha =$ between -5° and 5° . We simulated target fixation by computing pupil coordinates for a set of 3–17 targets. Target positions varied between -15° and 15° horizontally and vertically, and were distributed across

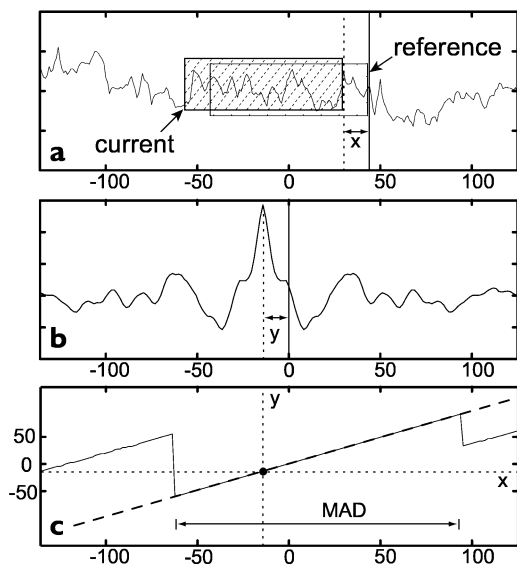


Fig. 2. Calculation of the MAD. (a) Iral signature pattern. The hollow box contains the reference pattern, the striped box the current data pattern. The horizontal displacement of the data versus reference pattern is the x coordinate for (c), representing actual ocular torsion (vertical displacement added for clarity). (b) The cross-correlation function of the two patterns in a. The position of the main peak yields the y -coordinates for (c). This corresponds to an actual measurement of ocular torsion based on the two patterns. (c) Measured versus actual torsion (i.e., main peak position versus window displacement). The solid dot represents the configuration shown in (a) and (b). Ideal measurement would yield a diagonal $y = x$, indicated by the dashed line. With realistic patterns, however, measured torsion will jump to a false value at some critical torsion angle. This is due to additional maxima of the cross-correlation exceeding the main maximum in size. The MAD is the torsional range over which measurement is stable.

the four quadrants. Only one of the targets was within a 1° radius of the straight ahead position.

These pupil coordinates and the corresponding angular target directions were used to obtain the calibration parameters as described above. Using these calibration parameters we then simulated gaze measurements during fixations: to simulate the fixations we computed pupil positions for 100 random directions between $\pm 15^\circ$ horizontally and vertically; and to simulate the measurement, we used these calculated pupil positions and the calibrated parameters to reobtain fixation angles by solving (4). The quality of the calibration was determined from the mean sum of the squared errors in horizontal and vertical fixation angles

$$\mathcal{E} = \sqrt{\frac{\sum_{i=1}^n (\Delta_\theta^2 + \Delta_\phi^2)}{n}}. \quad (8)$$

When the fixations in our simulations were accurate, \mathcal{E} was below 0.01° for any number of fixation targets. To get a more realistic estimate of the performance of the algorithm, fixation errors were added to the target fixation. Actual fixation angles of the simulated subjects were distributed normally around the targets ($\sigma = 0.5^\circ$). No fixation error was added to the simulated measurements, since the noise introduced by fixation errors would mask the errors due to incorrect calibration. To achieve a mean error $\leq 0.2^\circ$, 10–15 fixation points were required. A larger number of fixation points yielded no further improvement Fig. 3(a).

B. MAD Versus Autocorrelation

A distinct structure in an iral signature pattern often leads to a narrow, well pronounced peak of its autocorrelation function, while an indis-

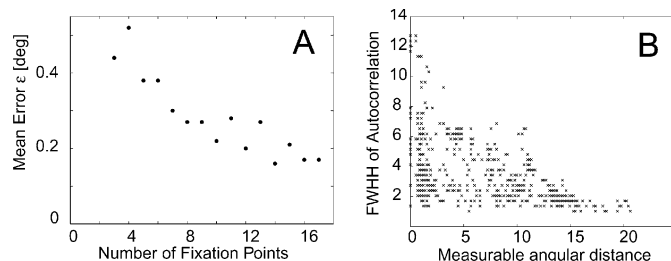


Fig. 3. (a) Mean squared error of parameter determination and position measurement, as defined in (8), for varying numbers of fixation targets. $\pm 0.5^\circ$ of fixation error were added to simulated fixations in calibration, but not in measurement (see text for details). (b) Comparison between FWHH (full width at half maximum) of the peak of the autocorrelation function and the MAD for a large random selection of patterns in a single image of the eye. Each dot represents one pattern.

tinct iral signature results in a wide peak. This is often used as an intuitive approach to the selection of iral patterns. To quantify this approach, we compared a pattern's MAD with the full-width at half-maximum (FWHM) of the central peak of its autocorrelation. We randomly extracted 1032 iral signature patterns from eye images taken with a 3-D VOG system manufactured by SensoMotoric Instruments. The images were 768×572 pixels in size. Pixels were sampled using a smoothing algorithm that took the weighted average of the nine pixels surrounding the exact image position to avoid aliasing. Patterns spanned 45° and had a length of 262 pixels.

We computed the MAD and the FWHM for each of these patterns and found that while there is a tendency for patterns with a large MAD to have narrow peaks of the autocorrelation function, the opposite is not true: there are many patterns with narrow peaks but poor values of the MAD Fig. 3(b).

V. DISCUSSION

A. Two-Dimensional (2-D) Calibration

Many scientific paradigms evaluate only horizontal or vertical eye movements. For such single-axis movements the center of eye rotation stays fairly constant, making the calibration easy: a simple sine-fit is sufficient to establish a correlation between pupil position in the image plane and the rotation angle of the eye. While for combined horizontal–vertical eye movements a consideration of the variable center of eye rotation is recommended, it becomes essential for 3-D eye position measurements: in the determination of torsional eye position, even small errors in the horizontal–vertical eye position measurement can induce large errors in the indicated torsional eye position [8]. Note that the calculation of the different parameters in the calibration procedure is not influenced by the choice of technique for the next step of the image analysis, i.e., for determining ocular torsion.

B. Pattern Selection

Different techniques have been used to determine the amount of ocular torsion: researchers have tracked retinal patterns [12], distinct landmarks on the iris [5], [11], artificial markers that have been painted on the sclera with food dyes [2], or iral signatures, i.e., light-dark patterns on a circle around the pupil [8], [9]. All these techniques need parameters that are provided by a calibration procedure like the one outlined above. A new and interesting approach to determine ocular torsion is the use of a mathematical neural network, as proposed and implemented by P. Guillemant and coworkers [6]. However, due to the lack of information about algorithms and implementation, it is hard to compare this approach with other techniques.

The iral-signature technique has the advantage that it is possible to quantify the suitability of selected patterns. Also, it is possible to use multiple patterns on opposite sides of the pupil center to correct for small mistakes in the pupil center determination [5]. Since ocular torsion determined from individual iral patterns can be quite susceptible to errors, e.g., if the pupil contracts or expands, it can be helpful to use a large number of iral patterns, and then statistically analyze the different amounts of torsion indicated by the individual iral signatures.

Our comparison of FWHM and MAD shows that the intuitive approach of picking patterns with a narrow peak of the autocorrelation function has its pitfalls. Online computation of the MAD for all relevant iral signature patterns and the selection of the best patterns based on this, is computationally expensive and would likely take too much time to be practical. Since all the patterns with a large MAD turned out to have a narrow peak of the autocorrelation function, an automated pattern selector could scan the image for patterns with narrow peaks of the autocorrelation function. Once a set of such patterns has been found, the MAD can be used to single out the ones best suited for torsion measurement.

The biggest remaining problems for VOG measurements are translations of the camera with respect to the head, and the influence of a change in pupil diameter on measuring the position of the pupil center. For VOG systems to replace scleral search coils, these have to be overcome.

ACKNOWLEDGMENT

The authors would like to thank C. Hårdter and D. B. Tweed for valuable comments on the manuscript.

REFERENCES

- [1] J. E. Bos and B. de Graaf, "Ocular torsion quantification with video images," *IEEE Trans. Biomed Eng.*, vol. 41, pp. 351–7, Apr. 1994.
- [2] A. Clarke, A. Engelhorn, C. Hamann, and U. Schonfeld, "Measuring the otolith-ocular response by means of unilateral radial acceleration," *Ann. N Y Acad. Sci.*, vol. 871, pp. 387–91, May 1999.
- [3] H. Collewijn, J. van der Steen, L. Ferman, and T. Jansen, "Human ocular counterroll: Assessment of static and dynamic properties from electromagnetic scleral coil recordings," *Exp. Brain Res.*, vol. 59, no. 1, pp. 185–96, 1985.
- [4] G. A. Fry and W. W. Hill, "The center of rotation of the eye," *Amer. J. Optom.*, vol. 39, no. 11, pp. 581–95, 1962.
- [5] E. Groen, J. E. Bos, P. F. M. Nacken, and B. de Graaf, "Determination of ocular torsion by means of automatic pattern recognition," *IEEE Trans. Biomed Eng.*, vol. 43, pp. 471–9, May 1996.
- [6] "Guillemant," Polytechnic Univ. Sch. Marseille (CNRS UMR), Marseille, France, <http://www.uratek.com/research/>, 2002.
- [7] T. Haslwanter, "Mathematics of three-dimensional eye-movements," *Vis. Res.*, vol. 35, no. 12, pp. 1727–39, 1995.
- [8] T. Haslwanter and S. T. Moore, "A theoretical analysis of three-dimensional eye position measurement using polar cross-correlation," *IEEE Trans. Biomed Eng.*, vol. 42, pp. 1053–61, Nov. 1995.
- [9] M. Hatamian and D. Anderson, "Design considerations for a real-time ocular counterroll instrument," *IEEE Trans. Biomed Eng.*, vol. 30, no. BME-5, pp. 278–88, May 1983.
- [10] S. T. Moore, T. Haslwanter, I. S. Curthoys, and S. T. Smith, "A geometric basis for measurement of three-dimensional eye position using image processing," *Vis. Res.*, vol. 36, no. 3, pp. 445–59, 1996.
- [11] K. Nakayama, "Photographic determination of the rotational state of the eye using matrices," *Amer. J. Optom. Physiol. Opt.*, vol. 51, no. 10, pp. 736–42, Oct. 1974.
- [12] D. Ott, F. Gehle, and R. Eckmiller, "Video-oculographic measurement of 3-dimensional eye rotations," *J. Neurosci Methods*, vol. 35, no. 3, pp. 229–34, Dec. 1990.
- [13] R. Peterka and D. Merfeld, "Calibration techniques for video-oculography," *J. Vestib. Res.*, vol. 6, no. 4S, p. 75, 1996.
- [14] D. A. Robinson, "A method of measuring eye movement using a scleral search coil in a magnetic field," *IEEE Trans. Biomed. Electron.*, vol. 10, pp. 137–45, 1963.
- [15] K. Schreiber, "Erstellung Und Optimierung Von Algorithmen Zur Messung Von Augenbewegungen Mittels Video-Okulographie-Methoden," Master's thesis, Universität Tübingen, Tübingen, Germany, 1999.
- [16] L. Stark, *Neurological Control Systems; Studies in Bioengineering*. New York: Plenum Press, 1968, ch. 3.
- [17] J. van der Geest and M. Frens, "Recording eye movements with video-oculography and scleral search coils: A direct comparison of two methods," *J. Neurosci. Methods*, vol. 114, no. 2, pp. 185–95, Mar. 2002.
- [18] H. Wyatt, "The form of the human pupil," *Vis. Res.*, vol. 35, no. 14, pp. 2021–36, July 1995.
- [19] D. Zhu, "Video-Based Approach for Tracking Eye Orientation in Three Dimensions," Ph.D. dissertation, Grad. Sch. The Univ. New York, New York, 1997.
- [20] D. Zhu, S. Moore, and T. Raphan, "Robust pupil center detection using a curvature algorithm," *Comput. Methods Programs Biomed.*, vol. 59, no. 3, pp. 145–57, June 1999.

Ellipsoidal Refinement of the Regularized Inverse: Performance in an Anatomically Realistic EEG Model

Paul H. Schimpf*, Jens Haueisen, and Ceon Ramon

Abstract—Functional brain imaging and source localization based on the scalp's potential field requires a solution to the inverse electrostatic problem. This is an underdetermined problem with many solutions. Minimum norm and regularization methods involving the norm are often used, but generally give solutions in which current is widely distributed. One method for reducing the spatial distribution of a solution is to apply it iteratively within the bounds of a shrinking ellipsoid. This paper compares the performance of this approach with an exhaustive search at various noise levels using a numeric simulation of the electroencephalogram in a realistic conductor model. The results show that inverting a single dipolar source with a location accuracy comparable to an exhaustive search requires in the range of 5 to 10 dB higher signal-to-noise ratio.

Index Terms—EEG, finite element, head model, inverse method, minimum norm, regularization, source localization.

I. INTRODUCTION

The localization of current sources in the brain from the electroencephalogram (EEG) requires a solution to the inverse electrostatic problem, which is defined as the determination of current sources from a partial observation of the potential field, in this case limited to a set of locations on the scalp. The so-called "lead-field" approach to this problem requires the assembly of a matrix, \mathbf{L} , which captures the linear relationship between the observed potentials and each possible dipolar source location and orientation [1]. Assembling the matrix \mathbf{L} requires a solution to the Poisson equation for each possible source

Manuscript received March 13, 2003; revised August 10, 2003. This work was supported in part by the National Science Foundation (NSF) under Grant 9726712 and Grant 0112742. Asterisk indicates corresponding author.

*P. H. Schimpf is with the School of Electrical Engineering and Computer Science, Washington State University, Spokane, WA 99202 USA (e-mail: schimpf@wsu.edu).

J. Haueisen is with the Biomagnetic Center, Friedrich-Schiller-University Jena, 07743 Jena, Germany.

C. Ramon is with the Department of Electrical Engineering, University of Washington, Seattle, WA USA.

Digital Object Identifier 10.1109/TBME.2004.824141